Supporting Information

Hu et al. 10.1073/pnas.1307574110

SI Materials and Methods

RNA Isolation and Real-Time qPCR. Total RNA isolation from cultured cells and freshly isolated human retinal pigment epithelial (RPE) cells, RNA quality assessment, cDNA reverse transcription, and qPCR were as previously described (1). qPCR was performed using the Bio-Rad CFX96 Realtime PCR Detection System (Bio-Rad). Melt curves for each pair of primers were inspected to confirm a single amplicon. The C_t values were normalized to a housekeeping gene (acidic ribosomal phosphoprotein P0, 36B4). Gene-expression fold changes were calculated using the ΔΔCT method. Primer sequences used were selected from Primer Bank, http://pga.mgh.harvard.edu/primerbank and are presented in Table S4.

Electrophoresis and Immunoblotting. Whole-cell protein extracts and RPE/choroid scraped from the posterior of mouse eyes were prepared using RIPA buffer [50 mM Tris·HCl (pH 7.5), 150 mM NaCl, 1% Nonidet P-40, 0.5% sodium deoxycholate, 0.05% SDS, 1 mM EDTA, and protease inhibitors (Sigma)]. Total protein concentrations were determined (Pierce BCA Protein Assay; Thermo Scientific). Proteins (15-25 μg per well) were separated with Bio-Rad Mini Protean-TGX precast gel systems, transferred onto nitrocellulose membranes, and detected using antibodies listed in Table S5 and appropriate secondary antibodies (Jackson Immunoresearch) (2). Densitometric analyses of protein bands in the Western blots were performed using Image J software from the National Institutes of Health. Relative band intensities were used to calculate the integrated optical density for each band, and then each band was normalized with the integrated optical density of the corresponding housekeeping protein band. For secreted protein, loading volume was normalized with respective protein values.

Immunohistochemistry and Morphology. For immunohistochemistry, eyes were fixed in 4% paraformaldehyde, cryopreserved (2), and cryosectioned from the superior cup through the optic nerve to the inferior cup in 10-μm increments. Cryosections randomly selected from the nasal, temporal, and central regions of the eye were probed with antibodies against retinal markers listed in Table S5. Nonspecific immunostaining in cryosections was blocked with normal serum (Jackson Immunoresearch) appropriate to the secondary antibody species. Secondary antibodies were conjugated to Alexa 568 and 488 (Invitrogen). Control slides containing sequential sections were probed with nonimmune serum and buffer without primary antibody. Hoechst 33258 was used to stain nuclei. For lectin labeling, sections were incubated with rhodamine-conjugated peanut agglutinin (PNA, *Arachea hypogea* agglutinin). Images were collected on a Nikon C1 confocal microscope. Percent staining area/entire area was measured throughout the RPE/choroid of the full eyecup in a minimum of three sections randomly selected from the nasal, temporal, and central regions of the eye. For electron microscopy, eyes were fixed in 2% gluteraldehyde, postfixed in 1% osmium tetroxide, and embedded in Spurrs resin. Morphology of the retina/RPE/choroid was studied in 1 μm toluidine blue-stained plastic sections. Inner nuclear layer and outer nuclear layer thicknesses were measured at 1,200 μm from the optic nerve head. Incidence of pathology in aryl hydrocarbon receptor ($AhR^{-/-}$) eyes, including RPE abnormalities (seen in greater than 20% of the eye), presence of sub-RPE deposits, retinal and choroidal neovascularization, and thickness of Bruch's membrane, were evaluated in electron microscopy thin sections (n = 6–10 images per mouse, n = 11–12 mice per genotype were examined). Eyes were graded as having focal (minimum of five rounded deposits confined to an area below one to two RPE cells) and diffuse deposits (confluent deposits covering more than 20% below the RPE).

Analysis of ERG recordings. Rod-driven a-waves were measured at 8 ms after the flash stimulus was applied, and cone-driven a-waves were measured at 14 ms after the flash, respectively [to exclude postreceptoral contribution from the analysis (3)]. For b-wave amplitude determination, the oscillatory potentials were removed from the signals by 55-Hz low-pass frequency filtering, and the b-wave amplitude was calculated from the bottom of the a-wave response to the b-wave peak. Averaged b-wave amplitudes were plotted as a function of flash intensity. The resulting stimulus-response curves were fitted to Eq. **S1** using a least-square fitting procedure (Scientist Software; MicroMath):

$$R = R_{\max,1}\frac{I^{n_1}}{I^{n_1}+I_{0.5,1}^{n_1}} + R_{\max,2}\frac{I^{n_2}}{I^{n_2}+I_{0.5,2}^{n_2}}. \qquad [S1]$$

The first and second terms of Eq. **S1** describe rod- and cone-driven responses, respectively, usually observed at flash intensities ≥ ~0.5 cd·s/m^2 for dark-adapted mice (4). $R_{\max,1}$ and $R_{\max,2}$ are maximal response amplitudes, n_1 and n_2 are Hill coefficients, and $I_{0.5,1}$ and $I_{0.5,2}$ are the half-saturating flash intensities. Stimulus-response curves were obtained under photopic conditions, and the data points from a-wave stimulus-response curves were fitted to a single term of Eq. **S1**.

Complement Factor H (CFH) genotyping of RPE cells. Because a single nucleotide polymorphism in CFH has been identified to confer risk for AMD (5–8), we genotyped all of our human samples. Wild-type (WT) individuals carry two 402Y alleles with no increased risk for age-related macular degeneration (AMD). Heterozygotes carry one 402Y and one 402H allele and have an approximate fourfold increased risk for AMD compared with WT. Homozygotes carry two 402H alleles and have an approximate 12-fold increased risk for AMD compared with WT. RPE cDNA was amplified by using ReadyMix Taq PCR reagent (Sigma). Two hundred nanograms of cDNA was used as template DNA in 40 μL of PCR. PCR conditions were as follows: 1 cycle for 30 s at 94 °C, 40 cycles for 30 s at 94 °C, 30 s at 55 °C, and 20 s at 72 °C, with an extension for 5 min at 72 °C. The PCR product is 127 bp. Twenty microliters of the PCR amplification product was digested by the restriction enzyme NlaIII at 37 °C for 4 h followed by heat inactivation of the enzyme at 67 °C for 20 min. Polyacrylamide gel electrophoresis (PAGE) was used to determine CFH genotype. Precast PAGE gels (Bio-Rad) were used. After electrophoresis, the gels were stained with SYBR Gold nucleic acid gel stain (Invitrogen) for 40 min and then visualized under UV light.

Rd8 genotyping. DNA was extracted from $AhR^{-/-}$ mice tails by using DirectPCR Lysis Reagent (Viagen Biotech). Tails from C57BL/6N mice, which carry the Rd8 mutation (gift from Cathy Bowes Rickman, Durham, NC; original source Charles River) served as a positive control. The rd8 genotype was tested by PCR with RED Taq ReadyMix PCR Mix (Sigma-Aldrich). The sequences of primers used were as follows: mCrb1 mF1, GTGAAGACAGCTACAGTTCTGATC; mCrb1 mF2, GCCCCTGTTTGCATGGAGGAAACTTGGAAGACAGCTACAGTTCTTCTG; mCrb1 mR, GCCCCATTTGCACACTGATGAC (9).

Each mouse sample was checked for both wild-type allele and rd8 mutation allele by using two individual PCR reactions. The primers mCrb1 mF1 and mCrb mR were used for wild-type allele, and the amplified product was 220 bp. The primers mCrb1 mF2 and mCrb mR were used to identify the rd8 allele, and the amplified product was 244 bp. The PCR parameters were as follows: 1 cycle for 3 min at 94 °C, 33 cycles for 30 s at 94 °C, 30 s at 63 °C, and 1 min at 72 °C, with an extension for 7 min at 72 °C. The PCR products were identified on a 3% agarose gel.

Cigarette smoke extract (CSE). CSE was prepared as previously described (10). In brief, the smoke from two research grade cigarettes (University of Kentucky, Tobacco Health Research) were bubbled through 20 mL of serum-free DMEM/F12, and the resulting suspension was then filtered through a 0.20-μm pore filter to remove bacteria and large particles. The resulting CSE was evaulated for nicotine content. Batches of CSE were normalized based on the nicotine concentration. CSE was stored at −20 °C until use.

1. Dwyer MA, Kazmin D, Hu P, McDonnell DP, Malek G (2011) Research resource: Nuclear receptor atlas of human retinal pigment epithelial cells: potential relevance to age-related macular degeneration. *Mol Endocrinol* 25(2):360–372.
2. Malek G, Li CM, Guidry C, Medeiros NE, Curcio CA (2003) Apolipoprotein B in cholesterol-containing drusen and basal deposits of human eyes with age-related maculopathy. *Am J Pathol* 162(2):413–425.
3. Robson JG, Frishman LJ (2004) Sampling and interpolation of the a-wave of the electroretinogram. *Doc Ophthalmol* 108(3):171–179.
4. Herrmann R, et al. (2010) Phosducin regulates transmission at the photoreceptor-to-ON-bipolar cell synapse. *J Neurosci* 30(9):3239–3253.
5. Edwards AO, et al. (2005) Complement factor H polymorphism and age-related macular degeneration. *Science* 308(5720):421–424.
6. Hageman GS, et al. (2005) A common haplotype in the complement regulatory gene factor H (HF1/CFH) predisposes individuals to age-related macular degeneration. *Proc Natl Acad Sci USA* 102(20):7227–7232.
7. Haines JL, et al. (2005) Complement factor H variant increases the risk of age-related macular degeneration. *Science* 308(5720):419–421.
8. Klein RJ, et al. (2005) Complement factor H polymorphism in age-related macular degeneration. *Science* 308(5720):385–389.
9. Mattapallil MJ, et al. (2012) The Rd8 mutation of the Crb1 gene is present in vendor lines of C57BL/6N mice and embryonic stem cells, and confounds ocular induced mutant phenotypes. *Invest Ophthalmol Vis Sci* 53(6):2921–2927.
10. Carp H, Janoff A (1978) Possible mechanisms of emphysema in smokers: In vitro suppression of serum elastase-inhibitory capacity by fresh cigarette smoke and its prevention by antioxidants. *Am Rev Respir Dis* 118(3):617–621.

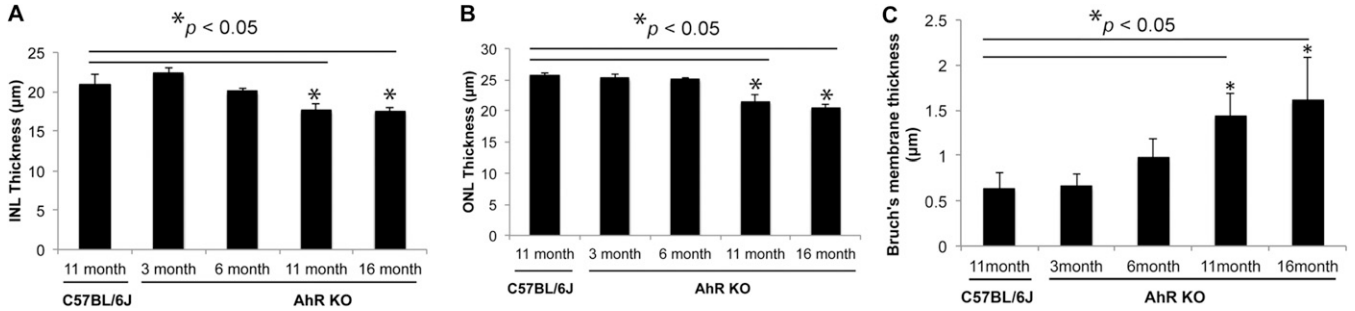

Fig. S1. Age-related changes in the photoreceptor and bruch's membrane thickness of 11-mo-old C57BL/6J and $AhR^{-/-}$ mice. Measurements of the (*A*) inner nuclear layer (INL) and (*B*) outer nuclear layer (ONL) thickness of photoreceptors, at 1,200 μm distance from the optic nerve head, as a function of age. (*C*) Measurement of Bruch's membrane thickness as a function of age. $n = 6$–10 images per mouse, $n = 11$–12 mice per genotype were examined. Data are means ± SEM. Statistical significance was analyzed with Student *t* test; $P < 0.05$.

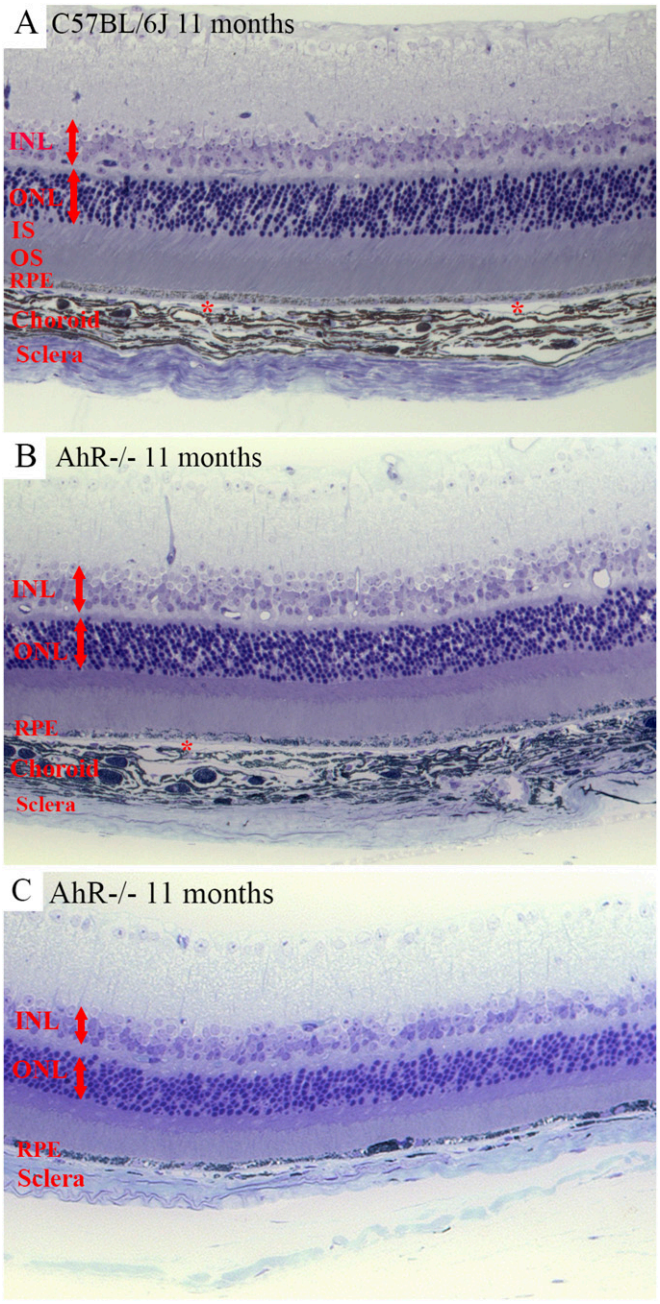

Fig. S2. Morphology of retina/RPE choroid and sclera of 11-mo-old C57BL/6J and $AhR^{-/-}$ mice spanning 1/5th the length of the total mouse eyecup. Morphology of retina/RPE in 1-μm-thick plastic sections stained with toluidine blue from a (*A*) 11-mo-old wild-type mouse, (*B* and *C*) 11-mo-old $AhR^{-/-}$ mice. INL, inner nuclear layer; ONL, outer nuclear layer; IS, inner segment of photoreceptors; OS, outer segment of photoreceptors; RPE, retinal pigment epithelium; asterisk, choriocapillaris. Double-headed red arrows show thickness of INL and ONL layers. n = 6–10 images per mouse, n = 11–12 mice per genotype were examined.

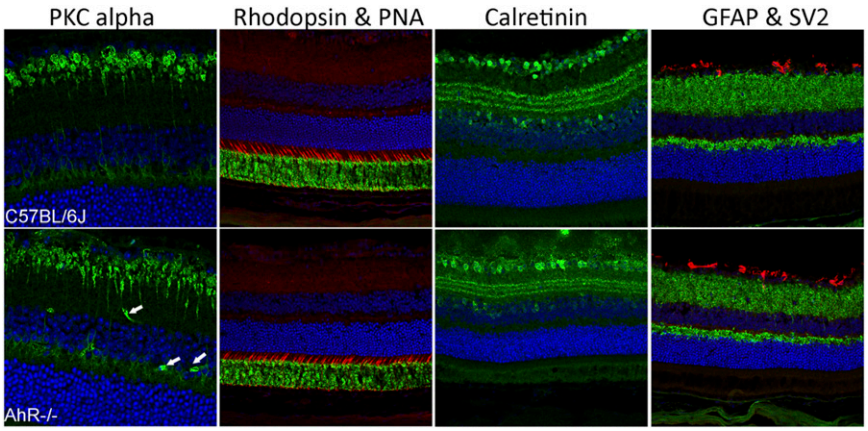

Fig. S3. Immunohistochemistry of retinal markers. Cryosections from 11-mo-old wild-type and *AhR*$^{-/-}$ mice probed with markers for rod biopolar cells [PKC alpha, protein kinase C alpha (green)], rhodopsin (green), cone photoreceptor sheath [PNA, peanut agglutinin (red)], inner plexiform cells (calretinin, green), glial cells [GFAP, glial fibrillary acidic protein (red)], and synaptic vesicles (SV2). Nuclei stained with Hoechst (blue). White arrows point to vessels in the inner retinal layers and not cells, which also appear green because the anti-PKC alpha antibody used was raised in a mouse. A minimum of three sections from the nasal, temporal, and central regions of the eye from $n = 5$ mice per genotype were stained and evaluated.

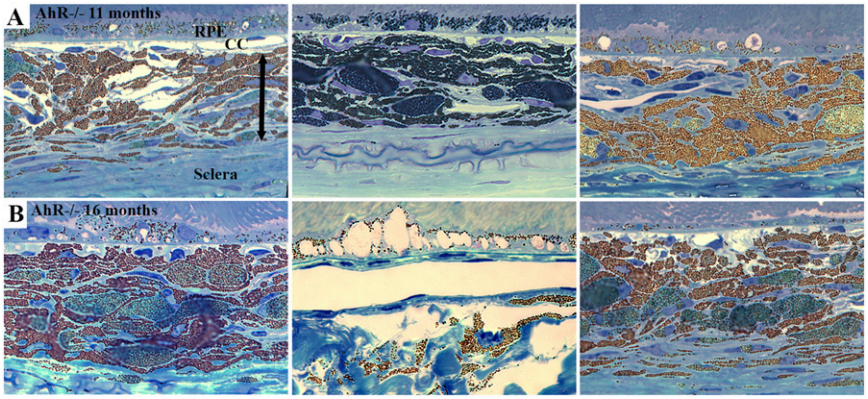

Fig. S4. Morphology of choroid in aged *AhR*$^{-/-}$ mice. (*A*) Eleven-month-old *AhR*$^{-/-}$ mice with diffuse and focal sub-RPE deposits and vacuolization as seen in Fig. 4*E*. CC, choriocapillaris; RPE, retinal pigment epithelium. Double-headed black arrow spans the choroid. (*B*) Sixteen-month-old *AhR*$^{-/-}$ mice, with considerable RPE pigmentary changes, extensive vacuolization, RPE atrophy, and depigmentation as seen in Fig. 4*F*. Here, the highly pigmented choroid associated with these RPE changes can be seen in further detail.

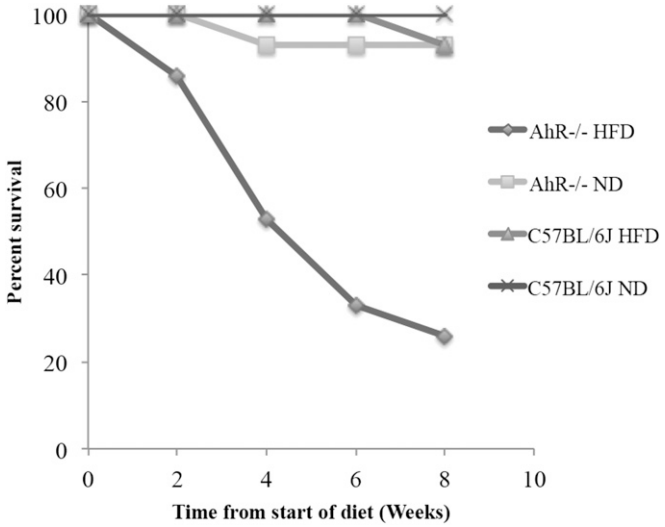

Fig. S5. Effect of diet on *AhR*$^{-/-}$ and C57BL/6J mice survival. Mice were fed a normal (ND) or high-fat diet (HFD) for 8 wk. Mortality of *AhR*$^{-/-}$ mice on high-fat diet increased progressively over the 8-wk period. However, survival rates of wild-type mice on the HFD and wild-type and *AhR*$^{-/-}$ on the ND remained high over the 8-wk dietary regimen. $n = 15$ per genotype per diet.

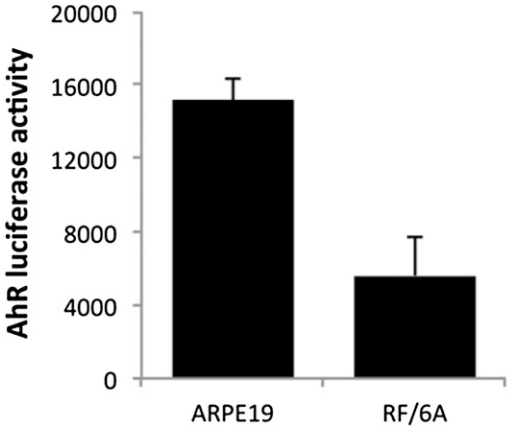

Fig. S6. AhR activity in RPE and choroidal endothelial cells. Endogenous AhR luciferase activity in RPE (ARPE19) and endothelial (RF/6A) cell culture lines. Each experiment was performed a minimum of three times. Data are means ± SEM.

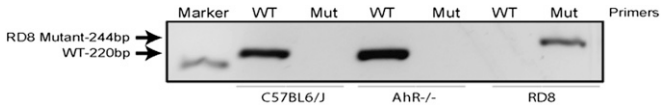

Fig. S7. Genotyping of *AhR*$^{-/-}$ mice for the RD8 gene. Agarose gel of DNA samples from C57BL/6J, *AhR*$^{-/-}$, and mice carrying the RD8 mutation using wild-type and mutant primers.

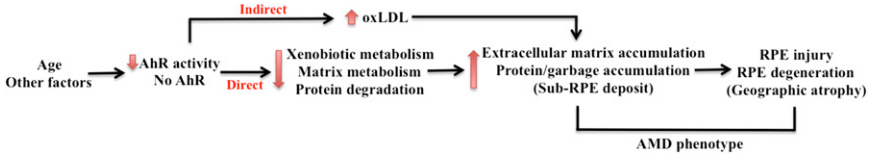

Fig. S8. Proposed molecular mechanism of AhR in AMD. With age, there is a decrease in RPE AhR activity resulting in a decrease in cellular xenobiotic metabolism and matrix metabolism. Decreased AhR activity may lead to increased extracellular accumulation of proteins and extracellular matrix molecules (sub-RPE deposits) as seen in early dry AMD and ultimately RPE degeneration as seen in geographic atrophy. Additionally, decreased AhR may lead to circulating lipoprotein levels, which can stimulate secretion of extracellular matrix molecules from RPE cells and further contribute to deposit accumulation.

Table S1. List of drugs, concentrations, and sources

Drugs	Concentration	Source
TCDD	10 nM	Sigma-Aldrich
CSE (cigarette smoke extract)	1.50%	Univ. of Kentucky/research grade cigarettes
HQ (hydroquinone)	75 μM	Sigma-Aldrich
BAP (benzo(*a*)pyrene)	1 μM	Sigma-Aldrich
βNF (beta-naphthoflavone)	100 nM	Sigma-Aldrich
αNF (alpha-napthoflavone)	100 nM	Sigma-Aldrich
AhR antagonist	1 μM	Calbiochem-182704
LDL (low-density lipoprotein)	50 μg/mL	Calbiochem
oxLDL (oxidized LDL)	50 μg/mL	Intracel

Table S2. Characteristic details of human samples

RPE cell line no.	Age of donor, y	Sex	CFH genotype
ARPE19	19	M	Heterozygote
159	7	F	WT
174	17	M	Heterozygote
106	31	M	WT
31	33	M	WT
160	51	F	Homozygote
115	58	M	Homozygote
154	61	M	Heterozygote
CM61	61	M	Homozygote
109	62	M	WT
66CF	66	F	Heterozygote
164	67	M	WT

Table S3. Incidence of AMD-related pathology in 11-mo-old *AhR*$^{-/-}$ and wild-type mice

		RPE changes				Sub-RPE deposits		Neovascularization	
Genotype	No. of eyes*	Hypo-pigmentation	Hyper-pigmentation	Loss of tight junctions	Atrophy	Focal	Diffuse	Retinal	Choroidal
AhR$^{-/-}$	12	11	10	12	12	5	12	0	0
C57BL/6J	11	0	2	1	0	0	0	0	0

Number of eyes with RPE changes >20% of the total length of the RPE. Focal deposits, rounded deposits underlying one-two RPE cells with a height >1/3 RPE height. Diffuse deposits, continuous deposits underlying several RPE cells.
*Number of eyes graded.

Table S4. List of primers

Gene	Primers	Sequence (5′→3′)
36B4	Forward	GGACATGTTGCTGGCCAATAA
	Reverse	GGGCCCGAGACCAGTGTT
AhR	Forward	TCCACCTCAGTTGGCTTTGTTTGC
	Reverse	TCGTGCACAGCTCTGCTTCAGTAT
ARNT	Forward	CCAACCAAGAAATGACATCAG
	Reverse	GTCGCCGCTTAATAGCCCTC
CYP1A1	Forward	TGCAGAAGATGGTCAAGGAG
	Reverse	AGCTCCAAAGAGGTCCAAGA
CYP1B1	Forward	CTGGATTTGGAGAACGTACCG
	Reverse	TGATCCAATTCTGCCTGCAC
Collagen IA1	Forward	GTGCTAAAGGTGCCAATGGT
	Reverse	ACCAGGTTCACCGCTGTTAC
Collagen IVa2	Forward	TCA CCA GGA CAG AAG GGA AG
	Reverse	CTC TGG CAC CTT TTG CTA GG
Laminin alpha 1	Forward	TGA AGA ATC GGA GGA ACT GG
	Reverse	CGC TTT CCC GTT AGA AAC AA
MMP2	Forward	GGTGCTCCACCACCTACAAC
	Reverse	CATAGGATGTGCCCTGGAAG
MMP14	Forward	CATTGGAGGAGACACCCACT
	Reverse	GAGGGGTCACTGGAATGCT
Fibronectin	Forward	ATGATGAGGTGCACGTGTGT
	Reverse	CTCTTCATGACGCTTGTGGA
Vitronectin	Forward	CACTATGCCGGAGGATGAGT
	Reverse	TCAGGATTCCCTTTGGACTG
TGFb	Forward	TTTTGATGTCACCGGAGTTG
	Reverse	GAACCCGTTGATGTCCACTT
SP1	Forward	GAAGGAGAAAACAGCCCAGA
	Reverse	AGCCTTGGATGTGGCAAATA

Table S5. Antibodies, sources, and applications

Application	Protein/label	Source	Dilution
Western blot	AhR	Santa Cruz	1:1,000
	CYP1A1	Santa Cruz	1:100
	CollagenIV	Abcam	1:10,000
	β-actin	Santa Cruz	1:5,000
	Fibronectin	Abcam	1:100
	TGF-β	Cell Signaling	1:100
IHC	Calbindin	SIGMA	1:2,000
	Calretinin	Chemicon	1:2,000
	Collagen IV	Millipore	1:30
	F/480	AbD Serotec	1:200
	GFAP	DAKO	1:100
	PKCα	Santa Cruz	1:200
	Rhodopsin	Chemicon	1:1,000
	SV_2	Hybridoma Bank	1:200
Lectin	PNA	Vector Laboratories	1:500